Materials Research Proceedings 54 (2025) 363-372 https://doi.org/10.21741/9781644903599-40

Significance of the material parameters within a three-dimensional solid-shell element for thermoforming simulation

Johannes Mitsch[1,a *], Bastian Schäfer[1,b] and Luise Kärger[1,c]

[1]Karlsruhe Institute of Technology (KIT), Institute of Vehicle System Technology (FAST) – Lightweight Engineering, 76131 Karlsruhe, Germany

[a]Johannes.Mitsch@kit.edu, [b]Bastian.Schaefer@kit.edu, [c]Luise.Kaerger@kit.edu

Keywords: Solid-Shell, Forming, Process Simulation, Finite Element Analysis (FEA)

Abstract. In this study, a hexahedral solid-shell element is employed for the simulation of the thermoforming processes for unidirectionally reinforced thermoplastic tapes. This allows for the direct application of a fully three-dimensional material behavior, in contrast to conventional two-dimensional approaches that neglect thickness deformations. However, the additional material parameters increase the computational effort during characterization. It is therefore crucial to distinguish the material parameters that have a significant influence on the final forming result from those that have a negligible impact. The results reveal that rate-dependent material modelling has the most significant influence on the final forming results. Therefore, it is crucial to accurately model the viscoelastic behavior to simulate thermoforming appropriately. Furthermore, the material parameters that describe the in-plane tension behavior are relevant for accurately predicting the material draw-in. The transverse shear stiffnesses for both the membrane and the bending behavior show low significance due to the low laminate thicknesses. Similarly, low bending stiffnesses, e.g., the elastic bending perpendicular to the fiber direction, are also of negligible significance compared to the high rate-dependency in those deformation modes.

Introduction

In the context of thermoforming process simulation for FRPs, the majority of macroscopic simulation approaches are based on two-dimensional shell elements [1]. Thermoplastic unidirectionally reinforced tapes typically have a high surface area relative to their thickness. Therefore, simulation approaches that employ conventional two-dimensional shell elements in a layered configuration are highly effective to accurately account for the membrane and bending deformation effects that occur during thermoforming as well as inter-ply interactions. A crucial aspect of thermoforming simulation is the decoupling of membrane and bending behavior within the intra-ply material behavior [2–4]. This is due to the high tensile stiffness in the fiber direction, while the stiffnesses perpendicular to the fiber direction, for shear deformation and bending deformation, are typically very small and are subject to a rate- and temperature-dependency [5,6].

The model developed by Schäfer et al. [7,8] employs a hexahedron solid-shell element which only has translational degrees of freedom. It is initially based on the work of Schwarze and Reese [9,10]. The model is suitable for anisotropic elastic materials and incorporates a membrane-bending decoupling into the formulation, thereby enabling an accurate prediction of the forming behavior of, e.g., non-crimp fabrics. In our previous study [11], we introduced a rate-dependent approach to enable modeling of viscoelastic material behaviors within the proposed solid-shell element.

In the current work, the solid-shell element proposed by Schäfer et al. [7,8] and Mitsch et al. [11] is employed for forming simulations. Compared to a two-dimensional approach, the hexahedral solid-shell approach requires higher computational costs due to the additional degree of freedom in thickness direction, the use of high-cost stabilization methods and the necessity for smaller time-step sizes. Consequently, characterization and parameterization routines that employ

the considered solid-shell approach are inherently time-consuming. It is therefore essential to identify the most impactful parameters for the forming simulation results, as only these parameters require characterization to accurately describe the in-plane and out-of-plane behavior within the solid-shell element. The remaining parameters can be approximated within their order of magnitude. Consequently, the sensitivity of the various material parameters regarding their influence on the final forming results within the thermoforming process are investigated.

Solid-Shell Element

Element formulation. In this study, a three-dimensional hexahedral solid-shell element is the focus of the analysis. This work is based on the research conducted by Schäfer et al. [11,12] and Mitsch et al. [13]. The element has eight nodes with only translational degrees of freedom. The implementation is realized as a user-element (VUEL) for ABAQUS/EXPLICIT. A reduced integration scheme is utilized for the in-plane deformations. Consequently, a single integration point is positioned at the center of the shell plane. Furthermore, the element incorporates multiple integration points distributed along its thickness, which facilitate the representation of the material behavior in the out-of-plane direction.

To prevent numerical locking, a variety of techniques are employed within the context of the solid-shell element. To prevent volumetric and Poisson thickness locking, the enhanced assumed strain (EAS) concept is employed [12–14]. It introduces an enhanced strain, $\boldsymbol{E}_{\mathrm{e}}$, which is added to the total compatible strain, $\boldsymbol{E}_{\mathrm{c}}(\boldsymbol{u}_i)$, which is solely dependent on the node displacements, $\boldsymbol{u}_i$. Furthermore, the assumed natural strain (ANS) concept is employed to prevent transverse shear and curvature thickness locking. This concept was introduced by Hughes and Tezduya [15]. Additional details on the implementation of the ANS and EAS concepts within the hexahedral solid-shell element are provided in [9,10,16].

Another essential aspect of the solid-shell user element is the separation of the membrane and the bending behavior. To this end, Taylor expansions of both the total strain $\boldsymbol{E}$ [9,10] and the resulting stress $\boldsymbol{S}$ [7] are employed. This allows for an independent description of the material behaviors associated with the membrane and the bending of the solid-shell element. As the methodology utilized within the solid-shell element was initially proposed for engineering textiles [11,12], the material behavior under consideration was constrained to elastic characteristics. Therefore, Mitsch et al. [11] enhanced the approach to a viscoelastic one, enabling the application of the proposed solid-shell element to pre-impregnated thermoplastic composites. A more comprehensive overview of the membrane-bending decoupling and the considered material behavior can be found in [7,11,17].

Viscoelastic material law. In this work, the behavior of a single layer of unidirectional reinforced tape is described through the utilization of a rate-dependent material law, the Voigt-Kelvin approach. The model represents the parallel connection of an elastic spring element with a viscous damper element. Consequently, the stresses $\boldsymbol{S}$ associated with the Voigt-Kelvin approach can be calculated additively [18]

$$\boldsymbol{S} = \boldsymbol{S}_{\mathrm{elast}} + \boldsymbol{S}_{\mathrm{visc}}, \tag{1}$$

where the elastic part $\boldsymbol{S}_{\mathrm{elast}}$ is described by the St. Venant-Kirchhoff model [19]

$$\boldsymbol{S}_{\mathrm{elast}} = \mathbb{C}[\boldsymbol{E}] \tag{2}$$

with the stiffness tensor $\mathbb{C}$ and the Green-Lagrange strain tensor $\boldsymbol{E}$. The viscous stresses $\boldsymbol{S}_{\mathrm{visc}}$ from Eq. 1 are modelled using the isotropic Newton model. Using the Newton model, the viscous Cauchy stress tensor $\boldsymbol{\sigma}_{\mathrm{visc}}$ is calculated by [20]

$$\boldsymbol{\sigma}_{\mathrm{visc}} = 2\eta\boldsymbol{D}, \tag{3}$$

Materials Research Proceedings 54 (2025) 363-372 https://doi.org/10.21741/9781644903599-40

where η is the scalar viscosity and $\boldsymbol{D}$ is the deformation rate tensor. Since the considered solid-shell element uses modifications of the total strain $\boldsymbol{E}$ based on the EAS and ANS concept, the deformation rate tensor $\boldsymbol{D}$ is not immediately available and has to be approximated. A routine to obtain an approximation for the deformation rate tensor $\boldsymbol{D}$ is given by Mitsch et al. [11].

The viscoelastic material behavior described by Eqs. 1-3 is applied separately to the membrane and bending behavior. To achieve this, a Taylor expansion is carried out for the resulting stresses and strain. This approach enables Eqs. 1-3 to independently characterize the membrane and bending behavior, with distinct material parameters for each. In particular, $\mathbb{C}_{\mathrm{M}}$ and η_{M} are used to characterize the membrane behavior, while $\mathbb{C}_{\mathrm{B}}$ and η_{B} are used to characterize the bending behavior. For a more detailed explanation of the derivation and calculation of the Taylor expansions mentioned, the reader is directed to references [7] and [11].

In the present study, Poisson ratios are not considered. This is due to the ratios of the selected membrane stiffness values (cf. Eq. 5), which yield negligible strains resulting from Poisson ratios. The Poisson ratios for the bending behavior lack physical meaning and can thus be omitted. As a result, the stiffness tensors describing the elastic membrane and bending behavior are diagonal when displayed in the fiber-oriented coordinate system and in Voigt notation

$$\mathbb{C}_{\mathrm{M}} \mathrel{\widehat{=}} \begin{bmatrix} C_{\mathrm{M}}^{11} & & & & & \\ & C_{\mathrm{M}}^{22} & & & & \\ & & C_{\mathrm{M}}^{33} & & & \\ & & & G_{\mathrm{M}}^{12} & & \\ & & & & G_{\mathrm{M}}^{23} & \\ & & & & & G_{\mathrm{M}}^{13} \end{bmatrix} \text{ and } \mathbb{C}_{\mathrm{B}} \mathrel{\widehat{=}} \begin{bmatrix} C_{\mathrm{B}}^{11} & & & & & \\ & C_{\mathrm{B}}^{22} & & & & \\ & & C_{\mathrm{B}}^{33} & & & \\ & & & G_{\mathrm{B}}^{12} & & \\ & & & & G_{\mathrm{B}}^{23} & \\ & & & & & G_{\mathrm{B}}^{13} \end{bmatrix}. \quad (4)$$

The elastic properties of the membrane are defined by $\mathbb{C}_{\mathrm{M}}$. The properties C_{M}^{11}, C_{M}^{22} and G_{M}^{12} describe the in-plane deformation behavior of the solid-shell element. In this context, the parameter C_{M}^{11} represents the stiffness of the solid-shell element, or alternatively the tape, in its fiber direction. In an analogous manner, C_{M}^{22} describes the stiffness perpendicular to the fiber direction. The parameter G_{M}^{12} describes the in-plane shear stiffness. The parameters C_{M}^{33}, G_{M}^{23} and G_{M}^{13} describe the out-of-plane stiffnesses of the membrane. In this context, C_{M}^{33} describes the compaction stiffness, while G_{M}^{23} and G_{M}^{13} describes the out-of-plane (transverse) shear stiffnesses of the membrane.

In the context of unidirectionally reinforced tapes, C_{M}^{11} is typically several orders of magnitude higher than the other stiffnesses components in $\mathbb{C}_{\mathrm{M}}$. However, selecting a physically accurate value for C_{M}^{11}, based on the stiffness of carbon or glass fibers, can lead to extremely small timesteps in explicit solvers. To balance accuracy and computational efficiency, C_{M}^{11} is often chosen lower than its physically measured value while remaining sufficiently high to approximate the fibers' inextensibility. This approach ensures that macroscopic forming simulations remain accurate while maintaining acceptable timesteps.

The elastic bending behavior is defined by $\mathbb{C}_{\mathrm{B}}$. The properties C_{B}^{11} and C_{B}^{22} describe the elastic bending behavior of the element in the direction of its element edges. Therefore C_{B}^{11} and C_{B}^{22} are bending stiffnesses in the fiber direction and perpendicular to it. The parameter C_{B}^{33} describes the correlation between compaction strains, which vary in thickness, and the corresponding stresses. The parameter G_{B}^{12} characterizes the elastic bending behavior in a direction diagonal to the element edges. The parameters G_{B}^{23} and G_{B}^{13} describe the stiffness corresponding to varying transverse shear strains over the thickness. Since no significant impact of the individual transverse shear stiffness ($G_{\mathrm{M}}^{23}, G_{\mathrm{M}}^{13}, G_{\mathrm{B}}^{23}$ and G_{B}^{13}) was determined in extensive parameter studies due to the small laminate thickness, these are summarized and referred to as G_{T} for both the membrane and the bending stiffnesses in the following.

Materials Research Proceedings 54 (2025) 363-372 https://doi.org/10.21741/9781644903599-40

Numerical Study

Numerical test setup. To ascertain the significance of a material parameter within the solid-shell element for the purposes of modelling and characterization, forming simulations are conducted with varying material parameters. The simulation setup is implemented in the commercially available finite element solver ABAQUS/EXPLICIT and is presented in Fig. 1. A hemispherical geometry (white) with diameter $d_\mathrm{P} = 150$ mm is employed for the punch. The die (red) is plane with a hole of diameter $d_\mathrm{D} = 160$ mm through which the blank (green) is formed. No blankholders are utilized to facilitate the evolution of wrinkles. The tools are modeled as discrete rigid surfaces. The forming process is implemented displacement-controlled by a Dirichlet boundary condition ($u_3 = 60$ mm) on the punch geometry, applied over one second. The die remains rigid in its initial position.

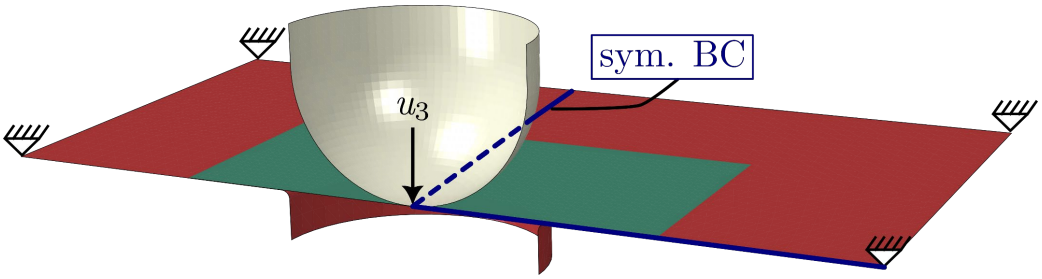

Figure 1 – Forming simulation setup for the hemisphere in ABAQUS/EXPLICIT adopted from [17]

The ply (green) is represented as a single layer of solid-shell elements, situated initially between the punch and the die (cf. Fig. 1). The ply itself represents a single layer of unidirectionally reinforced thermoplastic tape. The specimen's in-plane dimensions are 300 mm in length and 300 mm in width. The material exhibits a thickness of 0.3 mm. The length of the edges of the elements is 6 mm. As a result of the implementation of the problem's symmetry axes, only one quarter of the original problem needs to be simulated (blue lines), thereby reducing the overall simulation time. Consequently, the ply contains 625 hexahedral solid-shell elements. The contact between the tools and the ply is described using the General Contact definition from ABAQUS/EXPLICIT. The contact in the normal direction is described by a linear pressure-overclosure algorithm with a penalty stiffness and by Coulomb's friction law in the tangential direction with the coefficient of friction within the order of magnitude of values from literature [21], $\mu = 0.0644$.

The intra-ply material behavior of the ply is described using Eqs. 1-4. The elastic behavior is described using stiffness tensors $\mathbb{C}_\mathrm{M}$ and $\mathbb{C}_\mathrm{B}$ for the membrane and the bending behavior, respectively (cf. Eq. 4). Similarly, the rate-dependent behavior is described by isotropic viscosities, denoted as η_M and η_B. To facilitate the comparison of the relative significance of the different material parameters, a reference configuration of the material parameters is selected. Subsequently, the influence of the material parameters on the forming result is investigated by varying them. The parameter set for the membrane behavior in the reference configuration is selected as

$$\mathbb{C}_\mathrm{M}^\mathrm{ref} \mathrel{\widehat{=}} \begin{bmatrix} 1000.0 & & & & & \\ & 0.01 & & & & \\ & & 1.0 & & & \\ & & & 0.0035 & & \\ & & & & 1.0 & \\ & & & & & 1.0 \end{bmatrix} \text{MPa and } \eta_\mathrm{M}^\mathrm{ref} = 0.1\ \text{MPa} \cdot \text{s}. \tag{5}$$

The parameter set for the bending behavior in the reference configuration is selected as

Materials Research Proceedings 54 (2025) 363-372 https://doi.org/10.21741/9781644903599-40

$$\mathbb{C}_{\mathrm{B}}^{\mathrm{ref}} \mathrel{\widehat{=}} \begin{bmatrix} 75.0 & & & & & \\ & 0.75 & & & & \\ & & 0.01 & & & \\ & & & 0.375 & & \\ & & & & 1.0 & \\ & & & & & 1.0 \end{bmatrix} \text{MPa and } \eta_{\mathrm{B}}^{\mathrm{ref}} = 10\ \text{MPa} \cdot \text{s}. \tag{6}$$

The reference parameters were determined based on characterization experiments of glass-fiber reinforced polypropylene, with the same experimental setups as Dörr et al. [21]. However, constant viscosities are used to facilitate the parametric study, rather than the shear thinning that is typically observed for thermoplastic tapes. It should be noted that, with the exception of $\eta_{\mathrm{B}}^{\mathrm{ref}}$, which was found to be smaller in the present study compared to the experimental values reported in [21,22] for carbon fiber reinforced polyamide 6, all material parameters are in the same order of magnitude as those found in the referenced studies.

To examine the impact of the different material parameters on the final forming result, five sets of parameters were varied, according to Table 1. Thereby, the transverse shear as well as perpendicular and shear bending stiffness were varied simultaneously due to their individually negligible influence on the forming behavior, which will be discussed in the next Section.

Table 1 – Parameter variations to investigate significance during forming

	Increase	Decrease
Membrane viscosity	$\eta_{\mathrm{M}}^{+} = 2\ \eta_{\mathrm{M}}^{\mathrm{ref}}$	$\eta_{\mathrm{M}}^{-} = 0.1\ \eta_{\mathrm{M}}^{\mathrm{ref}}$
Bending viscosity	$\eta_{\mathrm{B}}^{+} = 10\ \eta_{\mathrm{B}}^{\mathrm{ref}}$	$\eta_{\mathrm{B}}^{-} = 0.1\ \eta_{\mathrm{B}}^{\mathrm{ref}}$
Transverse shear	$G_{\mathrm{T}}^{+} = 10\ G_{\mathrm{T}}^{\mathrm{ref}}$	$G_{\mathrm{T}}^{-} = 0.1\ G_{\mathrm{T}}^{\mathrm{ref}}$
Bending (fiber direction)	$C_{\mathrm{B}}^{11,+} = 10\ C_{\mathrm{B}}^{11,\mathrm{ref}}$	$C_{\mathrm{B}}^{11,-} = 0.1\ C_{\mathrm{B}}^{11,\mathrm{ref}}$
Bending (shear & perp. dir.)	$C_{\mathrm{B}}^{22,+} = 10\ C_{\mathrm{B}}^{22,\mathrm{ref}}$ $G_{\mathrm{B}}^{12,+} = 10\ G_{\mathrm{B}}^{12,\mathrm{ref}}$	$C_{\mathrm{B}}^{22,-} = 0.1\ C_{\mathrm{B}}^{22,\mathrm{ref}}$ $G_{\mathrm{B}}^{12,-} = 0.1\ G_{\mathrm{B}}^{12,\mathrm{ref}}$

It should be noted that a few material parameters have been held constant throughout the course of this study. The membrane stiffness C_{M}^{11} is not varied within this study since it represents the stiffness of the nearly strain-free fibers and is therefore selected to be comparatively high. The compaction stiffness C_{M}^{33} maintained at a constant value since it only affects the final thickness of the tape within the stamp-forming simulation and does not influence the formation of wrinkles during the forming process. The parameter C_{B}^{33} describes the correlation between compaction strains, which vary in thickness, and the corresponding stresses. Since these compaction strains lack physical significance and are solely a consequence of numerical considerations, the stiffness C_{B}^{33} is set to a value close to zero to prevent the induction of stresses or forces due to this deformation mode (cf. Eq. 6).

Results and discussion. The results of the forming process simulations are presented in Fig. 2. The displacements in the positive punch direction u_3 are represented using the red color bar, as these displacements correlate with the developed wrinkles within the laminate. In contrast, the displacement in the negative punch direction, u_3, is depicted as a uniformly blue, as these displacements are solely induced by the punch and are therefore not pertinent to this analysis. The forming result of the reference configuration is consistently displayed in the upper half of the visualizations. The forming results obtained using the varied parameter sets are illustrated in the lower half of the visualizations.

Fig. 2a shows the result of the forming simulation in the reference configuration. The outer contour demonstrates a considerably greater amount of material drawn in the 1-direction than in the 2-direction. This can be attributed to the fiber alignment in the 1-direction, which results in a significantly higher stiffness in this direction than in the 2-direction. Additionally, a total of twelve wrinkles were observed in the ply. The wrinkles situated at the ply edge in the 2-direction were observed to be deeper than those located at the edge in the 1-direction. This phenomenon can be attributed to more material draw-in in the 1-direction which geometrically increases the resistance against bending deformation. It can be concluded that the forming simulation for the reference configuration demonstrated the general expected result for the thermoforming process of a single ply.

Fig. 2b shows the influence of varied membrane viscosities. In comparison to the reference configuration, the introduction of a higher membrane viscosity (η_{M}^{+}) results in the formation of a greater number and depth of wrinkles. Similarly, when the membrane viscosity is decreased (η_{M}^{-}) the resulting deformed geometry was nearly flat, exhibiting minimal wrinkles. The observed behavior can be attributed to the fact that thermoplastic tapes exhibit two major deformation modes: in-plane shearing and out-of-plane bending. When shear deformation is prevented, for instance due to the laminate stack order or due to higher shear stiffness, bending deformation becomes more probable, leading to the formation of wrinkles. For $\eta_{\mathrm{M}} = \eta_{\mathrm{M}}^{+}$, shear deformation is prevented due to the higher viscous membrane stresses, which results in the formation of more and deeper wrinkles. Furthermore, Fig. 2b illustrates that an increased amount of material is drawn in the 2-direction in case of η_{M}^{+} compared to η_{M}^{-}. This is due to the deformation rates in the 2-direction, which induce higher viscous stresses with rising membrane viscosities. In the 1-direction, no such high deformation rates are observed due to the significantly higher elastic stiffness in fiber direction compared to the 2-direction.

Fig. 2c shows the impact of varied bending viscosities (cf. Table 1). In comparison to the reference configuration the increased bending viscosity (η_{B}^{+}) results in a reduction in the formation of wrinkles, whereas a decreased bending viscosity (η_{B}^{-}) results in an increase of wrinkles. Higher bending viscosities result in greater resistance to wrinkling, leading to increased shear deformation. This behavior is consistent with the results observed in Fig. 2b, as it represents the same effect in an inverse manner.

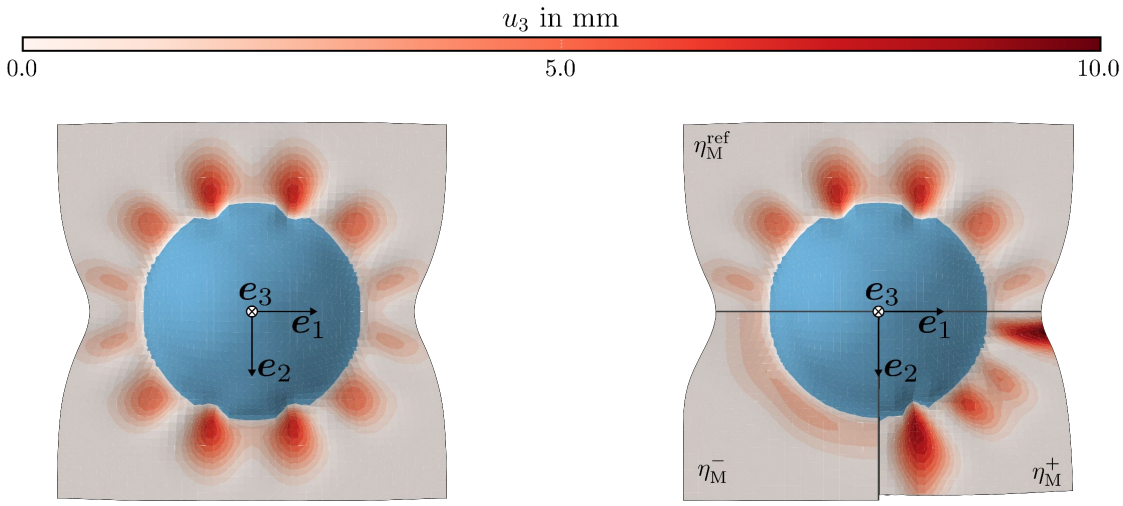

Subfigure 2a: Displacement field for the reference configuration

Subfigure 2b: Displacement field for varying membrane viscosities $\boldsymbol{\eta_M}$

Subfigure 2c: Displacement field for varying bending viscosities $\boldsymbol{\eta_B}$

Subfigure 2d: Displacement field for varying transverse shear stiffnesses $\boldsymbol{G_T}$

Subfigure 2e: Displacement field for varying bending stiffnesses $\boldsymbol{C_B^{11}}$ in fiber direction

Subfigure 2f: Displacement field for varying bending stiffnesses $\boldsymbol{C_B^{22}}$ and $\boldsymbol{G_B^{12}}$

Figure 2 – Simulation results for the forming problem

In Fig. 2d, the comparison between the reference configuration and the configuration utilizing varied transverse shear stiffnesses G_{T} for both the membrane- and the bending-behavior is shown (cf. Table 1). In contrast to Figs. 2b and 2c, neither significant variation in the formation of wrinkles nor notable discrepancies in the material draw-in are evident. This is due to the low laminate thickness (0.3 mm) and to the prevalence of rate-dependent material behavior. It can therefore be concluded that the elastic transverse shear stiffnesses for both the membrane- and the bending-behavior have an almost negligible influence on the forming results for similar parameter sets and equally small laminate thicknesses.

Fig. 2e shows the influence of varying bending stiffnesses in fiber direction C_{B}^{11} for the utilized elastic bending behavior (cf. Table 1). In the case of lower bending stiffnesses, the forming result exhibits only minor and insignificant differences. Conversely, in the case of higher bending stiffnesses, the maxima in u_3 were observed to shift to different locations. This is due to the higher ratio of resistance to bending deformation relative to the resistance to shear deformation, which is analogous to the results obtained in Fig. 2c. However, the small differences of the forming results in case of lower bending stiffnesses C_{B}^{11} cannot solely be explained with the ratio of bending and shear resistances. The minor discrepancies observed in the forming results for lower bending stiffnesses are expected to be attributed to the presence of considerable viscous stresses and forces, in comparison to the elastic stresses induced by the associated bending modes. Given that the deformation within this parameter range is predominantly governed by rate-dependent material behavior, a reduction in bending stiffness does not result in a significant alteration in the forming outcome.

This interpretation is corroborated by the findings presented in Fig. 2f, which shows the influence varying bending stiffnesses C_{B}^{22} and G_{B}^{12}. The forming results demonstrate that no notable discrepancies are evident in the presence of both increased and decreased bending stiffnesses. This can also be attributed to the markedly elevated viscous stresses and forces in this deformation mode relative to the elastic stresses induced by C_{B}^{22} and G_{B}^{12}. This finding aligns with the observations presented in Fig. 2e.

Conclusion and outlook

In this study, forming simulations of a single ply of thermoplastic tape are conducted. The material parameters that describe the rate-dependent material behavior and the transverse shear behavior are varied to ascertain their significance to the final forming result. Qualitative analyses based on the formation of wrinkles are performed to facilitate a comparison of the results.

The presented parameter study revealed that not all considered material parameters exert a significant influence on the final forming result. The transverse shear stiffnesses for both the elastic membrane and bending behavior have a negligible influence on the final forming result, which is due to the low ply thickness. Furthermore, the low bending stiffnesses also have a negligible influence on the final forming results, as the deformation is highly dominated by rate-dependent effects. It can be concluded that the modeling of these material parameters is not a crucial factor for the accurate prediction of wrinkles within thermoforming simulation utilizing the considered solid-shell element. However, these material parameters can contribute to the overall numerical stability of the model. Consequently, an appropriate selection of the transverse shear stiffnesses by means of numerical stability is valid within the solid-shell element.

The findings of this study indicate that an accurate modeling of the significant material properties of both the membrane and its bending behaviors is essential for an accurate prediction of wrinkles in thermoforming simulation. Moreover, the resulting negligible influence of the transverse shear stiffness and transverse bending stiffness are likely not limited to the specific case studied here as only a single ply of tape with comparably high thickness was considered. In multilayer composites, the influence of low stiffness values in the bending behavior would be

further diminished, as higher stiffness contributions from differently oriented layers would further reduce the effect of comparatively small stiffnesses.

Future studies will focus on enhanced modeling of the membrane and the bending behavior of thermoplastic tapes, e.g., by considering a deformation rate dependent viscosity model and considering temperature within the viscoelastic Voigt-Kelvin approach. Furthermore, thermoplastic composites usually consist of several layers with different orientations. Therefore, the goal of future work will also include the applicability of the solid-shell approach within a multilayer composite.

Acknowledgements
This work has been carried out in the DFG AI Research Unit 5339, funded by the Deutsche Forschungsgemeinschaft (DFG, German Research Foundation) – 459291153. The work is also part of the Heisenberg project 'Digitalization of fiber-reinforced polymer processes for resource-efficient manufacturing of lightweight components', funded by the DFG (project no. 455807141). The authors thank the German Research Foundation for its financial support.

References

[1] P. Bussetta, N. Correia, Numerical forming of continuous fibre reinforced composite material: A review, Composites Part A: Applied Science and Manufacturing 113 (2018) 12–31. https://doi.org/10.1016/j.compositesa.2018.07.010

[2] S.P. Haanappel, R.H.W. Thije, U. Sachs, B. Rietman, R. Akkerman, Formability analyses of uni-directional and textile reinforced thermoplastics, Composites Part A: Applied Science and Manufacturing 56 (2014) 80–92. https://doi.org/10.1016/j.compositesa.2013.09.009

[3] P. Boisse, N. Hamila, E. Vidal-Sallé, F. Dumont, Simulation of wrinkling during textile composite reinforcement forming. Influence of tensile, in-plane shear and bending stiffnesses, Composites Science and Technology 71 (2011) 683–692. https://doi.org/10.1016/j.compscitech.2011.01.011

[4] S. Allaoui, P. Boisse, S. Chatel, N. Hamila, G. Hivet, D. Soulat, E. Vidal-Salle, Experimental and numerical analyses of textile reinforcement forming of a tetrahedral shape, Composites Part A: Applied Science and Manufacturing 42 (2011) 612–622. https://doi.org/10.1016/j.compositesa.2011.02.001

[5] D. Dörr, F.J. Schirmaier, F. Henning, L. Kärger, A viscoelastic approach for modeling bending behavior in finite element forming simulation of continuously fiber reinforced composites, Composites Part A: Applied Science and Manufacturing 94 (2017) 113–123. https://doi.org/10.1016/j.compositesa.2016.11.027

[6] D. Dörr, T. Joppich, D. Kugele, F. Henning, L. Kärger, A coupled thermomechanical approach for finite element forming simulation of continuously fiber-reinforced semi-crystalline thermoplastics, Composites Part A: Applied Science and Manufacturing 125 (2019). https://doi.org/10.1016/j.compositesa.2019.105508

[7] B. Schäfer, D. Dörr, L. Kärger, Potential and challenges of a solid-shell element for the macroscopic forming simulation of engineering textiles, ESAFORM 2021 (2021). https://doi.org/10.25518/esaform21.883

[8] B. Schäfer, D. Dörr, L. Kärger, Reduced-Integrated 8-Node Hexahedral Solid-Shell Element for the Macroscopic Forming Simulation of Continuous Fibre-Reinforced Polymers, Procedia Manufacturing 47 (2020) 134–139. https://doi.org/10.1016/j.promfg.2020.04.154

[9] M. Schwarze, S. Reese, A reduced integration solid-shell finite element based on the EAS and the ANS concept-Geometrically linear problems, Int. J. Numer. Meth. Engng. 80 (2009) 1322–1355. https://doi.org/10.1002/nme.2653

[10] M. Schwarze, S. Reese, A reduced integration solid-shell finite element based on the EAS and the ANS concept-Large deformation problems, Int. J. Numer. Meth. Engng. 85 (2011) 289–329. https://doi.org/10.1002/nme.2966

[11] J. Mitsch, B. Schäfer, J.P. Wank, L. Kärger, Considering the viscoelastic material behavior in a solid-shell element for thermoforming simulation, in: Material Forming: ESAFORM 2024, Materials Research Forum LLC, 2024. https://doi.org/10.5445/IR/1000170492

[12] J.C. Simo, F. Armero, R.L. Taylor, Improved versions of assumed enhanced strain tri-linear elements for 3D finite deformation problems, Computer Methods In Applied Mechanics And Engineering 110 (1993) 359–386.

[13] J.C. Simo, F. Armero, Geometrically non-linear enhanced strain mixed methods and the method of incompatible modes, Int. J. Numer. Meth. Engng. 33 (1992) 1413–1449. https://doi.org/10.1002/nme.1620330705

[14] J.C. Simo, M.S. Rifai, A class of mixed assumed strain methods and the method of incompatible modes, Int. J. Numer. Meth. Engng. 29 (1990) 1595–1638. https://doi.org/10.1002/nme.1620290802

[15] T.J.R. Hughes, T.E. Tezduyar, Finite Elements Based Upon Mindlin Plate Theory With Particular Reference to the Four-Node Bilinear Isoparametric Element, J. Appl. Mech 48 (1981) 587–596. https://doi.org/10.1115/1.3157679

[16] M. Schwarze, I.N. Vladimirov, S. Reese, On the implementation of the EAS and ANS concept into a reduced integration continuum shell element and applications to sheet forming, Int J Mater Form 2 (2009) 919–922. https://doi.org/10.1007/s12289-009-0634-2

[17] B.B.J. Schäfer, Macroscopic forming simulation of unidirectional non-crimp fabrics: Hyperelastic material modeling and 3D-solid-shell approach, Dissertation, Karlsruher Institut für Technologie (KIT), 2024. https://publikationen.bibliothek.kit.edu/1000170739

[18] A. Bertram, Elasticity and Plasticity of Large Deformations: Including Gradient Materials, Springer, 2021.

[19] T. Belytschko, W.K. Liu, B. Moran, K.I. Elkhodary, Nonlinear finite elements for continua and structures, 2. ed., 1. publ, Wiley, Chichester, 2014.

[20] C.W. Macosko, Rheology: Principles, measurements, and applications, Wiley-VCH, New York NY u.a., 1994.

[21] D. Dörr, F. Henning, L. Kärger, Nonlinear hyperviscoelastic modelling of intra-ply deformation behaviour in Finite element forming simulation of continuously fibre-reinforced thermoplastics, Composites Part A: Applied Science and Manufacturing (2018). https://doi.org/10.1016/j.compositesa.2018.03.037

[22] D. Dörr, Simulation of the thermoforming process of UD fiber-reinforced thermoplastic tape laminates, Dissertation, Karlsruhe, 2019. https://doi.org/10.5445/IR/1000099485